Fast extraction of endmembers from convex simplex's boundary

ZHU Shulong, QI Jiancheng, ZHU Baoshan, CAO Wen

Department of Remote Sensing Information Engineering, Zhengzhou Institute of Surveying and Mapping, Henan Zhengzhou 450052, *China*

Abstract: Endmember extraction is one of the key problems for mixel classification of multispectral imagery. Existing algorithms based on convex simplex often find endmembers within the whole convex simplex so that their speeds are slower when more samples are used to obtain endmembers. Since only the vertexes of convex simplex are probably endmembers and they must be located in the boundary of convex simplex,the search space will shrink a lot if finding endmembers is performed only within the boundary points of convex simplex. According to this theory, this paper presents the endmember extraction algorithm based on the boundary of convex simplex. The algorithm includes determination of boundary of convex simplex and fast finding endmembers within the boundary points of convex simplex. Experiments show that the algorithm can find endmembers not only correctly but also faster than existing algorithms.

Key words: mixel, endmember, convex simplex, simplex's boundary, endmember extraction

CLC number: TP751.1 **Document code:** A

Citation format: Zhu S L, Qi J C, Zhu B S and Cao W. 2010. Fast extraction of endmembers from convex simplex's boundary. *Journal of Remote Sensing*. **14**(3): 482—492

1 INTRODUCTION

Mixel classification is one of the difficult problems in remotely-sensed image classification, in which endmember extraction is the key step that greatly affects the precision of mixel classification (Miao & Qi, 2007). Since convex simplex concepts were used in spectral unmixing of AVIRIS data by Boardman (1993), the methods based on convex simplex have been frequently used to extract endmenbers. For example, Pixel Purity Index (Boardman *et al.*, 1995) regards the pixel with the biggest Pixel Purity Index as an endmember. N-FINDR (Winter, 1999) and Simplex Growing Algorithm (Chang *et al.*, 2006) regard the vertexes of the simplex with the biggest volume as endmembers. Convex Cone Analysis (Ifarraguerri & Chang, 1999; CHU *et al.*, 2007) regards the pixel matched with the best vertexes of convex cone as an endmember. Sequential Maximum Angle Convex Cone (Gruninger *et al.*, 2004) regards the pixel with the biggest angle with respect to convex cone as an endmember. Vertex Component Analysis (Nascimento & Dias, 2005; Bajorski *et al.*, 2004) regards the extreme points as endmembers. Minimum Volume Transforms (Craig, 1994; Bowles *et al.*, 1998) regards the vertexes of simplex including all pixels and having the smallest volume as endmembers. Successive Projection Algorithm (Zhang *et al.*, 2008) regards the average spectrum of these pixels near vertexes of convex simplex as endmember's spectrum. The common characteristic of the above algorithms is finding endmembers within the whole convex simplex. In fact, only the vertexes of convex simplex are probably endmembers and the vertexes of convex simplex must be located on the boundary of convex simplex. Therefore, only from the boundary points of convex simplex, we can find endmembers very fast because the number of boundary points of convex simplex is much less than the number of all points within the whole convex simplex.

According to the above theory, the new endmember extraction algorithm, called Simplex Boundary Algorithm (abbreviated to "SBA"), is presented based on the boundary of convex simplex. It includes determination of boundary of convex simplex and fast finding endmembers within the boundary points of convex simplex. The comparison between SBA and N-FINDR is also performed for demonstrating the correctness and effectiveness of SBA.

2 EXTRACTION OF BOUNDARY OF CONVEX SIMPLEX

Because acquiring the boundary of high-dimensional convex simplex is much more difficult than two-dimensional convex simplex, it is necessary to represent the boundary of high-dimensional convex simplex using the boundary of two-dimensional convex simplex.

Let's firstly observe the relationship between endmembers in three-band images and boundary of two-dimensional convex simplex. If any two bands of the images are expressed graphically in a two-dimensional spectral space, we can obtain three two-dimensional scatter diagrams as shown in Fig. 1, where the symbol "×" expresses the positions of endmember 1, 2, 3 and 4.

Fig. 1 illustrates that endmember 2, 3 and 4 are located on the boundary of the left "cloud of points", endmember 1, 2, 3

Received: 2009-04-22; **Accepted**: 2009-08-31

First author biography: ZHU Shulong (1964—), male, Professor. He received PhD degree from Zhengzhou Institute of Surveying and Mapping, China, in June 1997. His research interests include remotely-sensed image processing, pattern recognition and digital photogrammetry. E-mail: zhushulong@sina.com

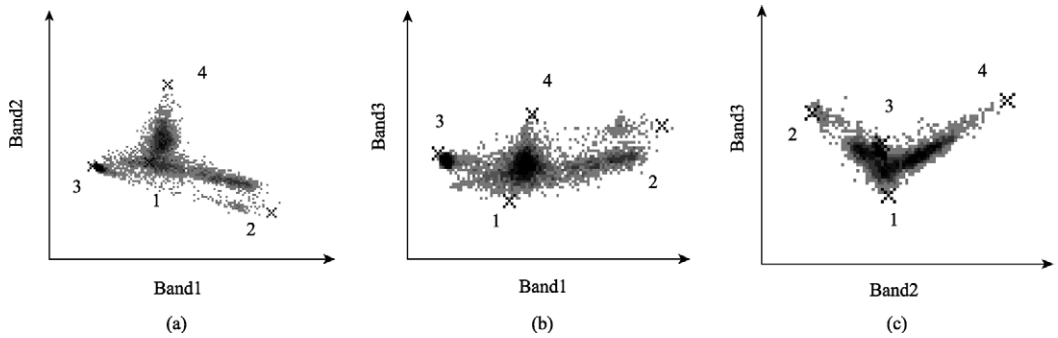

Fig. 1 Positions of endmenbers in two-dimensional scatter diagrams

and 4 in the middle, and endmember 1, 2 and 4 on the right. Although some endmembers are not located on boundary of "cloud of points", they are all in the union of all boundaries of three two-dimensional "clouds of points". Therefore all endmembers can be found from this union, that is, the boundary of three-dimensional convex simplex can be substituted by the union of all boundaries of these two-dimensional "clouds of points". It should be noted that the union of all boundaries of these two-dimensional "clouds of points" are only part of the boundary of high-dimensional convex simplex which includes all endmembers.

Generally, we can obtain C_{p-1}^2 two-dimensional scatter diagrams using (p–1) -band images only including p categories, each of which is generated using two bands of the images. We can also obtain the union of the boundaries of all C_{p-1}^2 two-dimensional "clouds of points" and further find p endmembers from the union. Next we need only the following algorithm to extract the boundary of two-dimensional "cloud of points" in two-dimensional coordinate system.

(1) Compute the minimum $x_{\min}$ and maximum $x_{\max}$ of horizontal coordinates of all points in two-dimensional "cloud of points".

(2) For $x\in[x_{\min}, x_{\max}]$, firstly find all points with the same x coordinate and then find the points with maximum or minimum y coordinate from it, which are regarded as a upper or lower boundary point, respectively.

(3) Compute the minimum $y_{\min}$ and maximum $y_{\max}$ of vertical coordinates of all points in two-dimensional "cloud of points".

(4) For $y\in[y_{\min}, y_{\max}]$, firstly find all points with the same y coordinate and then find the points with minimum or maximum x coordinate from it, which are regarded as a left or right boundary point, respectively.

(5) compute the union of all upper, lower, left and right boundary points, which is just the boundary of two-dimensional "cloud of points".

3 FAST EXTRACTION OF ENDMEMBERS FROM CONVEX SIMPLEX'S BOUNDARY

For m-band images only including p categories, where p is also the number of endmembers and $m\geqslant p$, we can obtain (p–1) principal component images after applying Principal Component Analysis (Keshava & Mustard, 2002) to it. We can further obtain the union of the boundaries of all C_{p-1}^2 two-dimensional "clouds of points" and can find p endmembers quickly from it.

Because the above algorithm for fast extracting endmembers is mainly based on simplex's boundary, it is called Simplex Boundary Algorithm (abbreviated to "SBA"). Next we describe SBA-algorithm in detail.

(1) If $m\geqslant p$, after applying PCA to m-band images only icluding p categories, (p–1) -band principal component images are obtained. And further C_{p-1}^2 two-dimensional scatter diagrams are acquired.

(2) Using two-dimensional simplex's boundary extraction algorithm, every boundary of C_{p-1}^2 two-dimensional "clouds of points" can be obtained. The union Π of all boundaries can be regarded as search space for finding endmembers in next steps.

(3) Pick p boundary points randomly from the union Π to constitute a set of initial endmembers expressed by $\left\{e_1^{(0)}, e_2^{(0)}, \ldots, e_p^{(0)}\right\}$.

(4) For $k\geqslant 0$, the volume of simplex with vertices $e_1^{(k)}, e_2^{(k)}, \ldots, e_p^{(k)}$ is calculated as follows

$$V\left(e_1^{(k)}, e_2^{(k)}, \ldots, e_p^{(k)}\right) = \frac{1}{(p-1)!}\mathrm{abs}\left(\begin{vmatrix} 1 & 1 & \cdots & 1 \\ e_1^{(k)} & e_2^{(k)} & \cdots & e_p^{(k)} \end{vmatrix}\right) \tag{1}$$

(5) For each boundary point in the union Π which is denoted by (p–1) -dimensional sample vector r, recalculate $V\left(r, e_2^{(k)}, \ldots, e_p^{(k)}\right)$, $V\left(e_1^{(k)}, r, \ldots, e_p^{(k)}\right)$, …, $V\left(e_1^{(k)}, e_2^{(k)}, \ldots, e_{p-1}^{(k)}, r\right)$, each of which is formed by replacing one endmember with r. Assume that $V\left(e_1^{(k)}, \ldots, e_{j-1}^{(k)}, r, e_{j+1}^{(k)}, \ldots, e_p^{(k)}\right)$ is the greatest of these p recalculated volumes and it is denoted by $V_{\max}$. If $V_{\max}$ is not

greater than $V\left(e_1^{(k)},e_2^{(k)},\ldots,e_p^{(k)}\right)$, then no endmember in $\left\{e_1^{(k)},e_2^{(k)},\ldots,e_p^{(k)}\right\}$ will be replaced. Otherwise the endmember $e_j^{(k)}$ in $\left\{e_1^{(k)},e_2^{(k)},\ldots,e_p^{(k)}\right\}$ is replaced with r and a new set of endmembers $\left\{e_1^{(k+1)},e_2^{(k+1)},\ldots,e_p^{(k+1)}\right\}$ is produced by letting $e_j^{(k+1)}=r$ and $e_i^{(k+1)}=e_i^{(k)}$ for $i\neq j$.

(6) The algorithm ends until every boundary point in the union Π are operated as above. The final set of endmembers is wanted.

Although SBA is similar to N-FINDR (Plaza & Chang, 2005) in the process of endmember extraction, N-FINDR finds endmembers from the whole convex simplex and SBA finds endmembers only from the boundary points of convex simplex. Therefore SBA is much faster than N-FINDR because its search space reduces a lot.

Fig. 2 The training images used for endmember extraction

4 EXPERIMENTS AND ANALYSES

In this section, SBA is compared with N-FINDR, a typical algorithm for endmember extraction, in order to demonstrate the correctness and effectiveness of SBA. And some important conclusions are also drawn from the following experiments.

4.1 Verification of SBA's correctness

In this experiment, the comparison between two groups of endmembers extracted by SBA and N-FINDR is conducted in order to demonstrate the correctness of SBA. The training images in this experiment are six-band subimages with the size of 200 pixels×200 pixels from Landsat-7 ETM+ images except the sixth band. The training images mainly include four categories: water, vegetation, bare soil and bare stone. Fig. 2 shows the composite image obtained using three bands of the training images.

Fig. 3 gives three two-dimensional scatter diagrams, each of them is generated using two of three principal components of the training images. The endmembers extracted by N-FINDR and SBA are represented by the symbol "⊙" and "×", respectively. The boundaries of "clouds of points" are represented by the symbol "·". Fig. 3 illustrates that two groups of endmembers extracted by SBA and N-FINDR are all located in the union of the boundaries of three "clouds of points". Fig. 3 also illustrates that endmembers extracted by SBA coincide with N-FINDR, respectively.

Table 1 lists the coordinates of four endmembers extracted by SBA and N-FINDR. Table 1 shows that the coordinates of every endmember extracted by SBA are the same as N-FINDR. This means the endmembers extracted by SBA are the same as N-FINDR. The correctness of four endmembers are also visually checked by plotting their positions on the image using the bright symbol "×" as shown in Fig. 2.

Although the endmembers extracted by SBA are the same as N-FINDR, there are 40000 pixels which are used as search samples in N-FINDR and only 676 pixels in SBA. Because the search space reduces a lot, the time consumption of SBA is much less than N-FINDR even if the time of boundary extraction is considered. Table 2 lists the time costs of N-FINDR and SBA, in which N-FINDR costs 672 ms to extract endmembers and SBA costs only 15 ms. SBA is much less than N-FINDR even if 172 ms of boundary extraction are included.

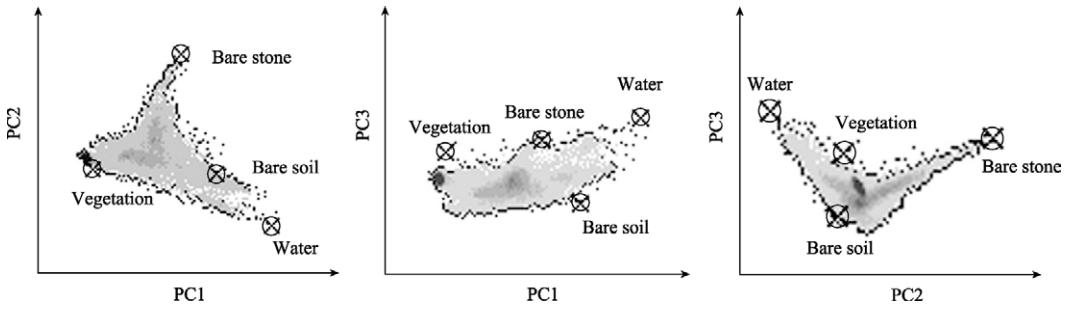

Fig. 3 Positions of endmembers and the boundaries of "clouds of points" in scatter diagrams

Table 1 Coordinates of endmembers obtained by N-FINDR and SBA

	Water	Vegetation	Bare soil	Bare stone
N-FIDNR	(101,120)	(172,54)	(185,195)	(136,165)
SBA	(101,120)	(172,54)	(185,195)	(136,165)

Table 2 The number of samples and the time consumption of N-FINDR and SBA

	N-FIDNR	SBA	
		Boundary extraction	Endmember searching
Number of samples	4×10^4	4×10^4	676
Time consumption /ms	672	172	15

4.2 The relationship between the speed of SBA and the number of endmembers

In this experiment, the subimages with the size of 400 pixels×350 pixels from 50-band AVIRIS hyperspectral images are used for endmember extraction. There are many categories in the subimages and their spectral resolution is 10nm and spectral range is 1.96—2.51μm. Fig. 4 shows the composite image of three bands of the subimages. Twenty-two groups of endmembers are extracted by SBA and N-FINDR for studying the relationship between the speed of SBA and N-FINDR and the number of endmembers. The number of endmembers in each group is from three to thirteen, respectively. Table 3 lists the time consumption of SBA and N-FINDR for different number of endmembers, where the time consumption of SBA includes the time of boundary extraction and endmember searching. Fig. 5 illustrates the relationship between the number of endmembers and the time consumption of SBA and N-FINDR. Fig. 6 illustrates the relationship between the number of endmembers and the ratio of time consumption of N-FINDR to SBA.

Table 3 and Fig. 5 show that the time costs of SBA and N-FINDR all increase rapidly while the number of endmembers increases, and SBA is always faster than N-FINDR. Table 3 and Fig. 6 show that the ratio of time consumption of N-FINDR to SBA is greater than 3.5 for any number of endmembers. However the ratio of time consumption of N-FINDR to SBA doesn't always increase. It firstly decreases and then increases while the number of endmembers increases. The turning point appears when the number of endmembers is 5 in this experiment. This study indicates that SBA has greater advantages than N-FINDR especially when more endmembers are extracted.

Table 3 Time consumption of SBA and N-FINDR for different number of endmembers

	Number of endmembers										
	3	4	5	6	7	8	9	10	11	12	13
N-FINDR /ms	1281	2156	3297	4954	7016	9391	13189	17641	22662	33891	42406
SBA /ms	312	578	938	1406	1969	2640	3438	4360	5437	6937	8360
Ratio of them	4.11	3.73	3.51	3.52	3.56	3.56	3.84	4.05	4.17	4.89	5.07

4.3 Relationship between the speed of SBA and the number of training samples

In this experiment, seven subimages with 10^3,5×10^3,10^4, 5×10^4,10^5,5×10^5 and 10^6 pixels are cut from Landsat-7 ETM+ images and used for endmember extraction. There are only four categories in every subimage. For each of the seven subimages, two groups of endmembers are extracted using SBA and N-FINDR, respectively. Table 4 records the time consumption of every extraction. Fig. 7 illustrates the relationship between the number of training samples and the time consumption of

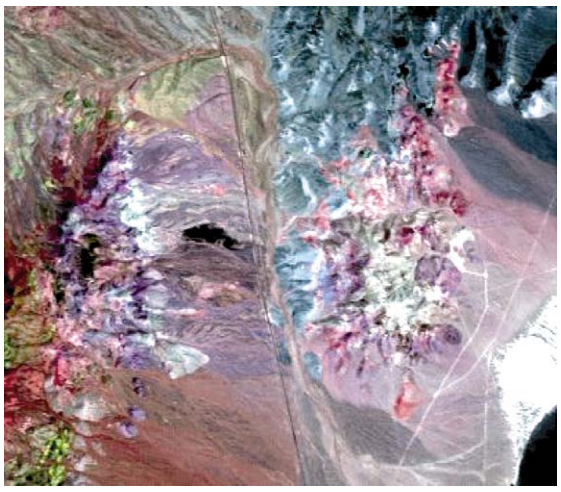

Fig. 4 AVIRIS composite image used for endmember extraction

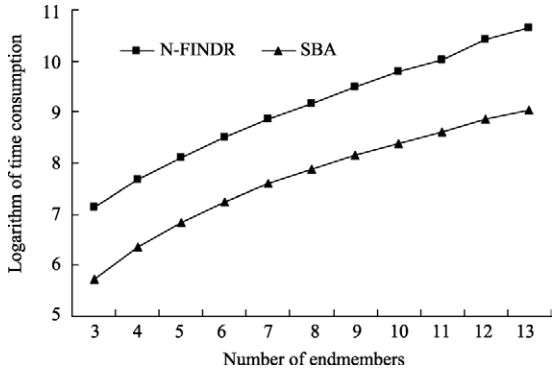

Fig. 5 Relationship between the number of endmembers and the time consumption

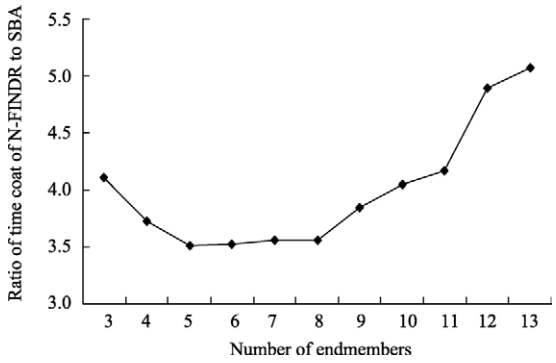

Fig. 6 Relationship between the number of endmembers and the ratio of time consumption of N-FINDR to SBA

SBA and N-FINDR. Fig. 8 illustrates the relationship between the number of training samples and the ratio of the time consumption of N-FINDR to SBA.

Table 4 and Fig. 7 show that the time costs of SBA and N-FINDR all increase rapidly while the number of training samples increases, and SBA is always faster than N-FINDR. Table 4 and Fig. 8 show that the ratio of the time consumption of N-FINDR to SBA is always greater than one for any size of the subimages, and it always increases. However, this increase becomes slower and slower when the number of training samples exceeds a value, for example 5×10^4 in this experiment. This study means that SBA has more advantages than N-FINDR when more training samples are used for endmember extraction.

Table 4 Time consumption of SBA and N-FINDR for different number of training samples

	Number of training samples						
	1	2	3	4	5	6	7
N-FINDR/ms	16	78	171	828	1672	8437	16875
SBA/ms	15	31	63	219	406	1969	3890
Ratio of them	1.07	2.52	2.71	3.78	4.12	4.28	4.34

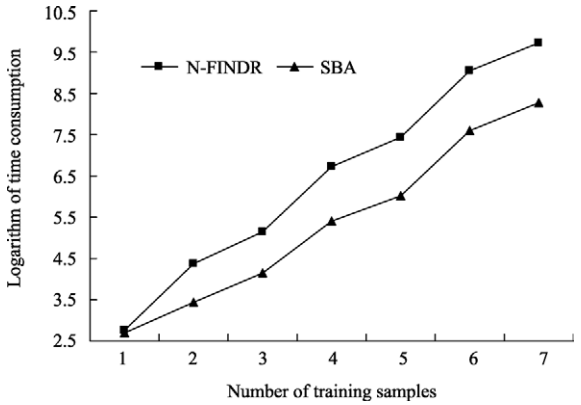

Fig. 7 Relationship between the number of training samples and the time consumption

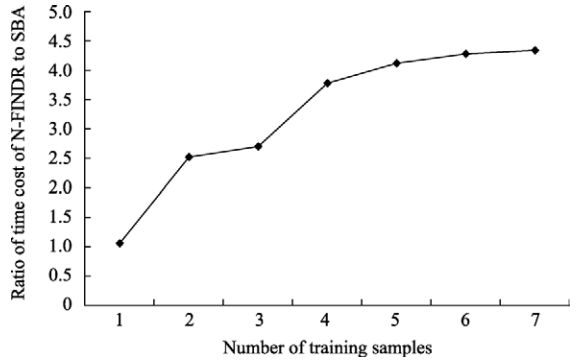

Fig. 8 Relationship between the number of training samples and the ratio of the time consumption of N-FINDR to SBA

5 CONCLUSIONS

(1) SBA can find all endmembers using the boundary of convex simplex as search space, and it can also finish endmember extraction with less time consumption because of less search space.

(2) Because all endmembers are in the union of all boundaries of two-dimensional "clouds of points", this union of boundaries can be used as search space in SBA algorithm, and all endmembers can be found from this union.

(3) With an increase of the number of endmembers or training samples, SBA has greater advantages in speed than N- FINDR.

REFERENCES

Bajorski P, Schott J and Ientilucci E. 2004. Comparison of basis-vector selection methods for target and background subspaces as applied to subpixel target detection. SPIE Proceeding, Algorithms and Technologies for Multispectral, Hyperspectral and Ultraspectral Imagery X

Boardman J W, Kruse F A and Green R O. 1995. Mapping target signatures via partial unmixing of AVIRIS data. Summaries of 5th Annual JPL Airborne Earth Science Workshop, Jet Propulsion Laboratory, Pasadena, CA, JPL Publication

Boardman J W. 1993. Automating spectral unmixing of AVIRIS data using convex geometry concepts. Summaries of 4th Annual JPL Airborne Geoscience Workshop, Jet Propulsion Laboratory, Pasadena, CA, JPL Publication

Bowles J, Daniel M, Grossman J, Antoniades J, Baumback M and Palmadesso P. 1998. Comparison of output from oasis and pixel purity calculations. SPIE Proceeding, Imaging Spectrometry IV, **3438**: 148—156

Chang C I, Wu C C, Liu W M and Ouyang Y C. 2006. A new growing method for simplex-based endmember extraction algorithm. *IEEE Transactions on Geoscience and Remote Sensing*, **44**(10): 2804—2819

Chu H F, Zhai Z M, Zhao Y D, Li P X and Zhang L P. 2007. A convex cone analysis method for endmember selection of multispectral and hyperspectral images, *Journal of Remote Sensing*, **11**(4): 460—467

Craig M D. 1994. Minimum volume transforms for remotely sensed data. *IEEE Transactions on Geoscience and Remote Sensing*, **32**(3): 542—552

Gruninger J, Ratkowski A J and Hoke M L. 2004. The sequential maximum angle convex cone(SMACC) endmember model. SPIE Proceeding, Algorithms for Multispectral, Hyperspectral and Ultraspectral Imagery, USA

Ifarraguerri A and Chang C I. 1999. Multispectral and hyperspectral image analysis with convex cone. *IEEE Transactions on Geoscience and Remote Sensing*, **37**(2): 756—770

Keshava N and Mustard J F. 2002. Spectral unmixing. *IEEE Signal Processing Magazine*, **19**(1): 44—57

Miao L D and Qi H R. 2007. Endmember extraction from highly mixed data using minimum volume constrained nonnegative matrix factorization. *IEEE Transactions on Geoscience and Remote Sensing*, **45**(3): 765—777

Nascimento J M P and Dias J M B. 2005. Vertex component analysis: A fast algorithm to unmix hyperspectral data. *IEEE Transactions on Geoscience and Remote Sensing*, **43**(4): 898—910

Plaza A and Chang C I. 2005. An improved N-FINDR algorithm in implementation. SPIE Proceeding, Algorithms and Technologies for Multispectral, Hyperspectral, and Ultraspectral Imagery XI, Bellingham, WA

Winter M E. 1999. N-FINDR: An algorithm for fast autonomous spectral endmember determination in hyperspectral data. SPIE Proceeding, Imaging Spectrometry V

Zhang J K, Rivard B and Rogge D M. 2008. The successive projection algorithm (SPA), an algorithm with a spatial constraint for the automatic search of endmembers in hyperspectral data. *Sensors*, (8): 1321—1342

以凸面单体边界为搜索空间的端元快速提取算法

朱述龙, 齐建成, 朱宝山, 曹 闻

解放军信息工程大学测绘学院遥感信息工程系 河南 郑州 450052

摘 要: 提出了以凸面单体边界为搜索空间的端元快速提取算法, 其核心包括凸面单体边界的确定和以凸面单体边界为基础的端元搜索两部分。实验表明: 该算法不仅能够准确地寻找到端元, 而且端元提取速度明显快于现有的端元提取算法。

关键词: 混合像元, 端元, 凸面单体, 单体边界, 端元提取

中图分类号: TP751.1 文献标识码: A

引用格式: 朱述龙, 齐建成, 朱宝山, 曹 闻. 2010. 以凸面单体边界为搜索空间的端元快速提取算法. 遥感学报, **14**(3): 482—492

Zhu S L, Qi J C, Zhu B S and Cao W. 2010. Fast extraction of endmembers from convex simplex's boundary. *Journal of Remote Sensing*. **14**(3): 482—492

1 引 言

混合像元分类是遥感图像分类的难点之一, 而端元提取是混合像元分类的关键, 它决定了混合像元分类精度的高低(Miao & Qi, 2007)。基于凸面单体(convex simplex)的端元提取方法, 是目前广泛采用的端元提取方法之一。其中主要算法有: Boardman(1993)最早提出的凸面单体端元提取算法; 把纯度指数最大的像元作为端元的像元纯度指数算法(Boardman 等, 1995); 把体积最大的单体顶点作为端元的 N-FINDR 算法(Winter, 1999)和单体生长算法(Chang 等, 2006); 把与凸锥最佳角点相匹配的像元作为端元的凸锥分析算法(Ifarraguerri and Chang, 1999; Chu 等, 2007); 把与凸锥夹角最大的像元作为端元的序贯最大角凸锥算法(Gruninger 等, 2004); 把投影极值点作为端元的顶点成分分析算法(Nascimento and Dias, 2005; Bajorski 等, 2004); 把体积最小且包含全部像元的单体顶点作为端元的最小体积变换算法(Craig, 1994; Bowles 等, 1998); 把凸面单体顶点附近具有空间连续性像元的平均光谱作为端元光谱的连续投影算法(Zhang 等, 2008)等。这些算法的共同特点是: 以整个凸面单体作为端元搜索空间, 且认为凸面单体内每个像元成为端元的概率是相同的。但事实上, 凸面单体内每个像元成为端元的概率是不同的, 由于凸面单体的顶点总是位于单体的边界上(此处“边界”是指二维凸面单体的边界线或高维凸面单体的表面), 所以仅从凸面单体的边界中搜索端元, 就可以找到端元。由于凸面单体边界所对应的像元数远小于凸面单体所对应的像元数, 因此仅从凸面单体的边界中搜索端元, 可以大大缩小端元搜索的范围, 加快端元提取的速度。

基于上述理由, 我们提出了以凸面单体边界为搜索空间的端元快速提取算法(简称为单体边界算法, 即 simplex boundary algorithm, 简写为 SBA 算法), 其核心包括凸面单体边界的确定和以凸面单体边界为基础的端元快速搜索两部分。为了验证 SBA 算法的正确性和有效性, 我们把 SBA 算法得到的端元以及 SBA 算法的端元提取效率, 与经典的 N-FINDR 端元提取算法进行了定量比较。

2 凸面单体边界的提取

由于高维凸面单体的形状比较复杂, 边界难以提取; 而理想的二维凸面单体为三角形(实际为二维特征点集), 边界点容易获取。所以需要首先解决用二维凸面单体边界表示高维凸面单体边界的问题。

收稿日期: 2009-04-22; 修订日期: 2009-08-31

第一作者简介: 朱述龙(1964—), 男, 1997 年 6 月在解放军测绘学院获博士学位, 教授、博士生导师。研究方向为遥感信息处理与应用、图像识别和数字摄影测量等。E-mail: zhushulong@sina.com。

先通过实验观察 3 个波段的多光谱影像中的端元(不妨假设端元数为 4)与二维凸面单体边界的关系。以其中任意两个波段为坐标轴分别构成二维特征空间，将对应波段的影像数据映射到该特征空间中，形成如图 1 所示的 3 个二维散点图(称为二维凸面单体)，其中端元是用 N-FINDR 算法确定的，分别为 1, 2, 3, 4，端元在二维散点图中的位置用“×”表示。在波段 1 和波段 2 构成的二维特征空间中，端元 2，3，4 处于散点图的边界；在波段 1 和波段 3 构成的二维特征空间中，端元 1，2，3，4 处于散点图的边界；在波段 2 和波段 3 构成的二维特征空间中，端元 1，2，4 处于散点图的边界。虽然有些端元可能不处于某一个二维散点图边界，但全部端元一定处于所有二维散点图边界的并集中。因此从二维散点图边界的并集中一定能够找出全部端元，即可以用所有二维散点图边界的并集代替高维凸面单体的边界，作为下一步端元搜索的范围。需要说明的是：二维散点图边界的并集，并不是严格意义上的高维凸面单体的边界，而是高维散点图(称为高维凸面单体)边界中包含端元的部分。

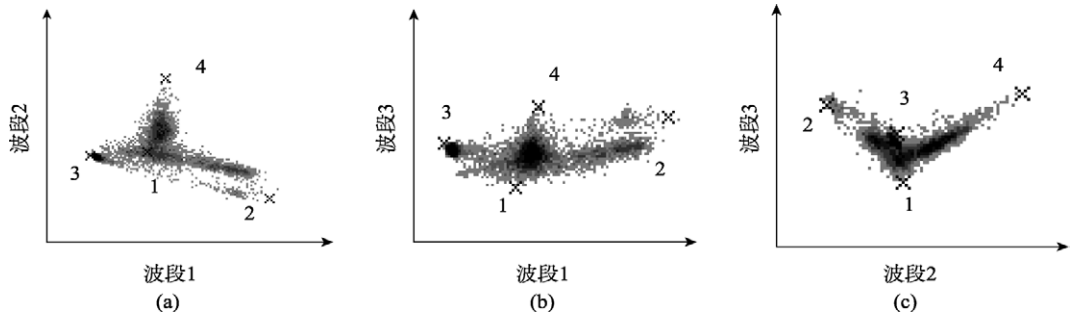

图 1 端元在二维散点图中的位置

对于包含 p 类地物 m 个波段的多光谱影像(即端元数为 p，且 $m \geqslant p$)，只要运用主成分分析算法(Keshava & Mustard, 2002)得到(p–1)个主分量影像，分别从中选取两个主分量影像构成 C_{p-1}^2 个二维特征空间，用全部 C_{p-1}^2 个二维特征空间中散点图边界的并集作为搜索空间，就可以从中找出 p 个端元。这样，高维凸面单体边界提取问题就转化为二维凸面单体边界的提取问题。下面给出二维凸面单体边界提取算法，基本思想是：分别在纵轴方向和横轴方向上搜索二维散点图的边界点，所有边界点的并集即为二维散点图的边界。算法的具体步骤如下:

(1) 计算二维特征空间中所有点的横坐标的最小值 $x_{\min}$ 和最大值 $x_{\max}$。

(2) 对于横坐标值相同的特征点，从中找出纵坐标值最大和最小的特征点，作为二维散点图的边界点；遍历 $x \in [x_{\min}, x_{\max}]$，得到二维散点图的上边界和下边界。

(3) 同样，计算二维特征空间中所有点的纵坐标的最小值 $y_{\min}$ 和最大值 $y_{\max}$。

(4) 对于纵坐标值相同的特征点，从中找出横坐标值最小和最大的特征点，作为二维散点图的边界点；遍历 $y \in [y_{\min}, y_{\max}]$，得到二维散点图的左边界和右边界。

(5) 求上、下、左、右边界的并集，就得到二维凸面单体的全部边界。

3 基于凸面单体边界的端元快速提取算法

对于包含 p 类地物 m 个波段的多光谱影像(即端元数为 p，且 $m \geqslant p$)，运用主成分分析算法(简写为 PCA 算法)和上一节的二维凸面单体边界提取算法，获得 C_{p-1}^2 个二维特征空间中散点图边界的并集。由于 p 个端元在该二维散点图边界的并集中，因此用全部 C_{p-1}^2 个二维特征空间中散点图边界的并集作为搜索空间，以凸面单体边界为搜索空间，从中找出 p 个端元。为此，我们提出以凸面单体边界为搜索空间的端元快速提取算法(简称 SBA 算法)，该算法描述如下:

(1) 指定端元数目为 p，利用 PCA 算法将训练影像的维数降至 p–1，用得到的主分量为轴构成 p–1 维影像特征空间，则影像在该特征空间中形成 p–1 维凸面单体。

(2) 运用本文提出的二维凸面单体边界提取方法，分别获得 p–1 维凸面单体对应的 C_{p-1}^2 个二维散点图边界，其并集Π作为下一步端元的搜索空间。

(3) 从并集Π中随机选择 p 个边界点作为候选端元。以候选端元为顶点构成 p–1 维凸面单体，按下式计算该单体的体积:

$$V_1 = \frac{1}{(p-1)!}\mathrm{abs}\left(\begin{vmatrix} 1 & 1 & \cdots & 1 \\ e_1 & e_2 & \cdots & e_p \end{vmatrix}\right) \quad (1)$$

式中，abs(*)表示求绝对值，|*|表示求行列式，e_j 表示第 j 个候选端元在 p–1 维影像特征空间中的光谱列向量。

(4) 对于并集Π中的某个边界点，将它依次临时取代这 p 个候选端元，以每次取代后的 p 个点为顶点构成 p–1 维凸面单体(共 p 个)，分别计算这 p 个单体的体积(计算方法同 V_1)，得到最大体积 V_2，并记录 V_2 对应的被取代的候选端元的编号(以 k 表示)。

(5) 若 $V_2 > V_1$，则将该边界点正式取代第 k 个候选端元；否则，保留原候选端元不变。

(6) 按照步骤(4)和(5)遍历并集Π中的每个边界点，最终保留下来的 p 个候选端元就是要寻找的 p 个端元。

SBA 算法与 N-FINDR 算法(Plaza & Chang, 2005)的端元提取过程类似，但 N-FINDR 算法从整个凸面单体中搜索端元，而 SBA 算法仅从凸面单体边界中搜索端元，从而大大缩小了端元搜索范围，能够大幅度提高端元提取速度。

4 实验及分析

为了验证 SBA 端元提取算法的正确性和效率，以 N-FINDR 端元提取算法为参照，将 SBA 与 N-FINDR 两种端元提取算法进行比较分析，得出以下结论。

4.1 SBA 算法所提端元的正确性检验

为了检验 SBA 算法所提端元的正确性，将 SBA 算法得到的端元与 N-FINDR 算法得到的端元进行一致性比较，对端元的正确性进行了目视判读检验。实验数据为某地区 Landsat-7 ETM+影像(实验中仅选用除热红外波段之外的 6 个波段图像)，从中选取 200×200 像元的影像作为训练样本，如图 2 所示(图 2 为其中 3 个波段的合成图像)，该影像主要包含水体、植被、土质裸地和石质裸地等 4 类地物(即端元数为 4)。

图 3 是采用图 2 训练影像的 3 个主分量分别形成的二维散点图，图中 N-FINDR 算法获取的端元用深色“⊙”表示，SBA 算法获取的端元用深色“×”表示，散点图边界用深色“·”表示。从图 3 可以看出: 两种算法得到的 4 个端元处于 3 个散点图边界的并集中，且两种算法得到的 4 对端元完全重合(端元在训练影像中的位置如图 2，其像元坐标见表 1)，目视判读也说明所提取的端元是正确的。这说明 SBA 算法与 N-FINDR 算法的结果是一致的、正确的。

图 2 用于端元提取的 ETM+训练影像

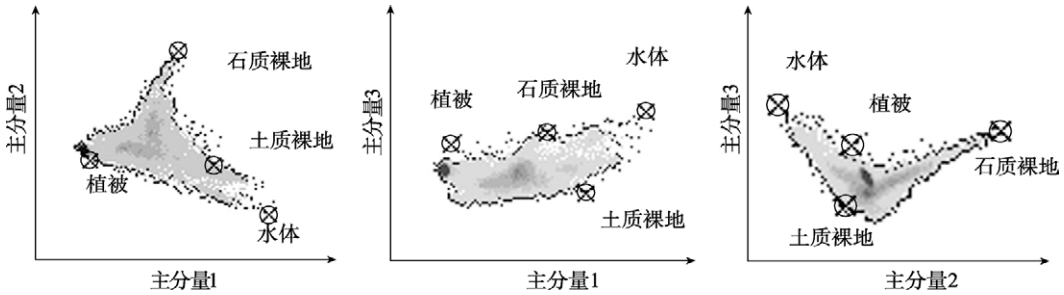

图 3 端元和边界在二维散点图中的位置

虽然 SBA 算法与 N-FINDR 算法可以获得相同的端元，但 N-FINDR 算法中参与端元搜索的样本有 4×10^4 个(即全部训练样本)；而 SBA 算法中参与端元搜索的样本仅有 676 个，搜索范围大大缩小，即使包括凸面单体边界提取时间，SBA 算法端元提取时间也比 N-FINDR 算法快很多，这正是 SBA 算法的优越性所在。表 2 列出了本实验中两种端元提取算法的时间花费，其中 N-FINDR 算法端元提取时间为 672ms，SBA 算法的边界提取时间为 172ms，端元搜索时间为 15ms，SBA 算法端元提取总时间为 187ms，远远少于 N-FINDR 算法端元提取时间 672ms。

表 1　N-FINDR 算法和 SBA 算法提取的端元的像元坐标

	水体	植被	土质裸地	石质裸地
N-FIDNR	(101,120)	(172,54)	(185,195)	(136,165)
SBA	(101,120)	(172,54)	(185,195)	(136,165)

表 2　参与 N-FINDR 和 SBA 的样本数目及对应的时间花费

	N-FIDNR	SBA	
		边界提取	端元搜索
样本数/个	4×10^4	4×10^4	676
时间/ms	672	172	15

4.2　SBA 算法的速度与端元数的关系

为了研究 SBA 算法的速度与端元数的关系，选择 50 个波段的 AVIRIS 高光谱影像(其光谱分辨率为 10nm,波长范围为 1.96－2.51μm，地物类别较多)，从中选取大小为 400×350 像元的影像作为训练样本，如图 4 所示(图 4 为其中三个波段的合成图像)。分别利用 SBA 算法和 N-FINDR 算法从该训练样本中提取 3, 4, …, 13 个端元，分别统计两种算法的时间花费(表 3，其中 SBA 算法包括凸面单体边界提取时间和端元搜索时间)，绘出两种算法端元提取时间与端元数之间的关系图(图 5，图 6)，分析两种算法端元提取时间与端元数之间的规律。由于 SBA 算法和 N-FINDR 算法所耗时间相差太大，为了在同一个坐标系中同时表达 SBA 算法和 N-FINDR 算法所耗时间随端元数变化的规律，我们以算法所耗时间的对数为纵坐标(以下类同)。

从表 3 和图 5 可以看出：随着端元数目的增多，SBA 算法和 N-FINDR 算法的时间花费显著增加，但 SBA 端元提取算法始终快于 N-FINDR 算法。从表 3 和图 6 看出：不论端元数的多少，N-FINDR 算法与 SBA 算法的时间比都在 3.5 倍以上，但是 N-FINDR 算法与 SBA 算法的端元提取时间之比，并不是单调递增的，而是随着端元数目的增多先减小后增大(实验中端元数为 5 时出现拐点)，特别是在端元数较大时，SBA 端元提取算法的速度优势更大。

4.3　SBA 算法的速度与训练样本数目的关系

为了研究 SBA 算法的速度与训练样本数的关系，我们从某地区 Landsat-7 的 ETM+影像(实验中仅选用除热红外波段之外的 6 个波段图像)上，分别选取像元数目为 10^3, 5×10^3, 10^4, 5×10^4, 10^5, 5×10^5, 10^6 的 7 个影像块作为训练样本(每个影像块只包含 4 类同样地物，由于篇幅的限制不再展示这些影像)，分别用 N-FINDR 算法和 SBA 算法从这 7 幅训练影像中提取 4 种端元，再分别统计两种算法的时间花费(表 4)，并绘出两种算法端元提取时间与训练样本数之间的关系图(图 7，图 8)，以此分析两种算法端元提取时间与训练样本数之间的规律。

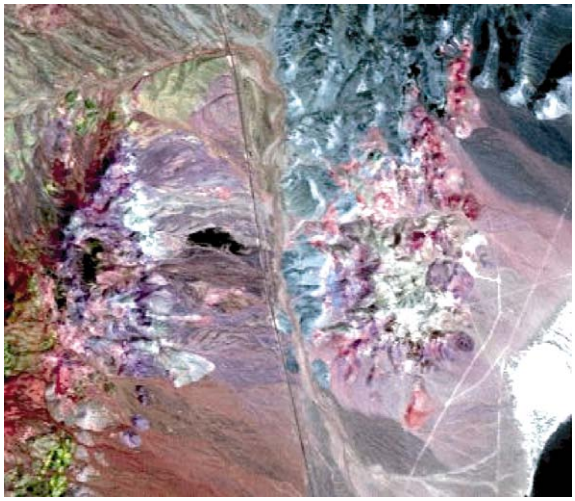

图 4　用于端元提取的 AVIRIS 训练影像

表 3　端元数目不同时 SBA 和 N-FINDR 的时间花费

	端元数目										
	3	4	5	6	7	8	9	10	11	12	13
N-FINDR/ms	1281	2156	3297	4954	7016	9391	13189	17641	22662	33891	42406
SBA/ms	312	578	938	1406	1969	2640	3438	4360	5437	6937	8360
时间花费之比	4.11	3.73	3.51	3.52	3.56	3.56	3.84	4.05	4.17	4.89	5.07

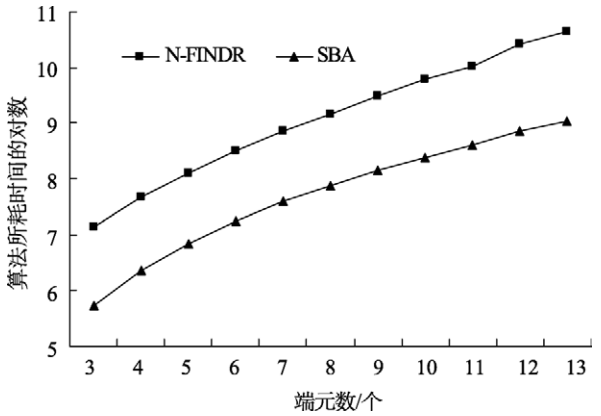

图 5　SBA 和 N-FINDR 所耗时间的对数与端元数的关系

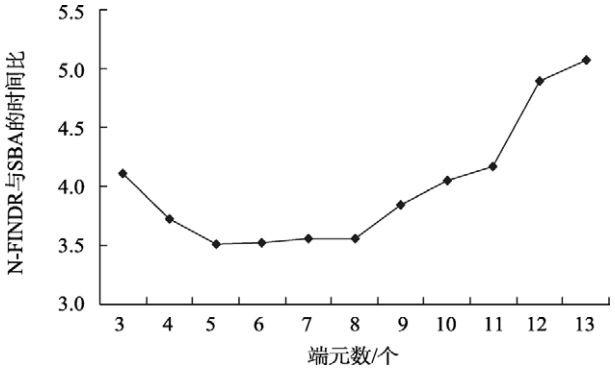

图 6　N-FINDR 和 SBA 的时间比与端元数的关系

表 4　训练样本数目不同时 **N-FINDR** 和 **SBA** 的时间花费

	训练样本数目						
	1	2	3	4	5	6	7
N-FINDR /ms	16	78	171	828	1672	8437	16875
SBA /ms	15	31	63	219	406	1969	3890
时间花费之比	1.07	2.52	2.71	3.78	4.12	4.28	4.34

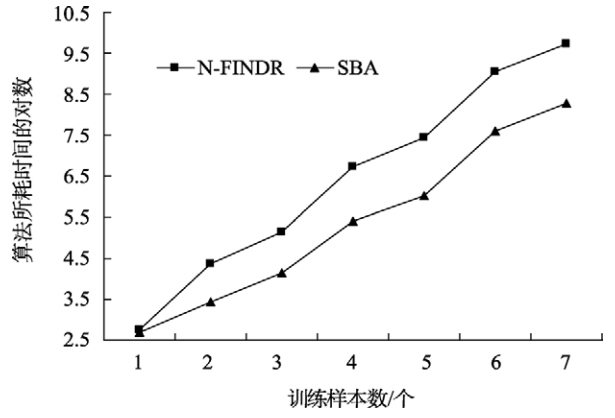

图 7　SBA 和 N-FINDR 所耗时间的对数与样本数的关系

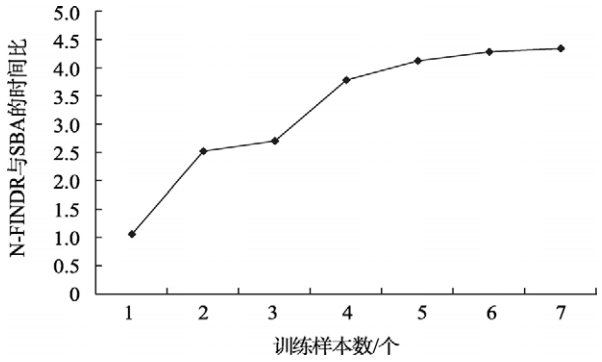

图 8　N-FINDR 和 SBA 的时间比与样本数的关系

由表 4 和图 7 可以看出: 随着训练样本数的增大, SBA 算法与 N-FINDR 算法的时间花费显著增加, 但 SBA 端元提取算法始终快于 N-FINDR 算法。由表 4 和图 8 看出: 不论训练样本数的多少, SBA 算法总是快于 N-FINDR 算法; 并且 N-FINDR 算法与 SBA 算法的端元提取时间之比随训练样本数的增多而增大, 是单调递增的, 因此当训练样本较多时, SBA 端元提取算法的速度优势更明显; 但是当训练样本数增大到一定程度(实验中训练样本数大于 5×10^4)时, 时间比增速趋缓, 稳定在 4—5 之间。

5　结　论

通过上述理论分析和实验研究, 可以得出如下结论:

(1) 基于凸面单体边界的端元提取算法(即 SBA 算法), 以训练样本所对应的特征空间中的凸面单体边界为端元搜索范围, 理论上一定能够找到端元, 并且由于端元搜索范围缩小很多, 端元提取速度要快很多。

(2) 在 SBA 算法中, 由于所有端元落在二维散点图边界的并集中, 因此用多个二维凸面单体边界的并集作为端元搜索范围是可行的, 且一定能够从中找出全部端元。

(3) 随着端元数、训练样本数的增加, SBA 算法的速度优势越来越显著。

REFERENCES

Bajorski P, Schott J and Ientilucci E. 2004. Comparison of basis-vector selection methods for target and background subspaces as applied to subpixel target detection. SPIE Proceeding, Algorithms and Technologies for Multispectral, Hyperspectral and Ultraspectral Imagery X

Boardman J W, Kruse F A and Green R O. 1995. Mapping target signatures via partial unmixing of AVIRIS data. Summaries of 5th Annual JPL Airborne Earth Science Workshop, Jet Propulsion Laboratory, Pasadena, CA, JPL Publication

Boardman J W. 1993. Automating spectral unmixing of AVIRIS data using convex geometry concepts. Summaries of 4th Annual JPL Airborne Geoscience Workshop, Jet Propulsion Laboratory, Pasadena, CA, JPL Publication

Bowles J, Daniel M, Grossman J, Antoniades J, Baumback M and Palmadesso P. 1998. Comparison of output from oasis and pixel purity calculations. SPIE Proceeding, Imaging Spectrometry IV, **3438**: 148—156

Chang C I, Wu C C, Liu W M and Ouyang Y C. 2006. A new growing method for simplex-based endmember extraction algorithm. *IEEE Transactions on Geoscience and Remote Sensing*, **44**(10): 2804—2819

Chu H F, Zhai Z M, Zhao Y D, Li P X and Zhang L P. 2007. A convex cone analysis method for endmember selection of multispectral and hyperspectral images, *Journal of Remote Sensing*, **11**(4): 460—467

Craig M D. 1994. Minimum volume transforms for remotely sensed data. *IEEE Transactions on Geoscience and Remote Sensing*, **32**(3): 542—552

Gruninger J, Ratkowski A J and Hoke M L. 2004. The sequential maximum angle convex cone(SMACC) endmember model. SPIE Proceeding, Algorithms for Multispectral, Hyperspectral and Ultraspectral Imagery, USA

Ifarraguerri A and Chang C I. 1999. Multispectral and hyperspectral image analysis with convex cone. *IEEE Transactions on Geoscience and Remote Sensing*, **37**(2): 756—770

Keshava N and Mustard J F. 2002. Spectral unmixing. *IEEE Signal Processing Magazine*, **19**(1): 44—57

Miao L D and Qi H R. 2007. Endmember extraction from highly mixed data using minimum volume constrained nonnegative matrix factorization. *IEEE Transactions on Geoscience and Remote Sensing*, **45**(3): 765—777

Nascimento J M P and Dias J M B. 2005. Vertex component analysis: A fast algorithm to unmix hyperspectral data. *IEEE Transactions on Geoscience and Remote Sensing*, **43**(4): 898—910

Plaza A and Chang C I. 2005. An improved N-FINDR algorithm in implementation. SPIE Proceeding, Algorithms and Technologies for Multispectral, Hyperspectral, and Ultraspectral Imagery XI, Bellingham, WA

Winter M E. 1999. N-FINDR: An algorithm for fast autonomous spectral endmember determination in hyperspectral data. SPIE Proceeding, Imaging Spectrometry V

Zhang J K, Rivard B and Rogge D M. 2008. The successive projection algorithm (SPA), an algorithm with a spatial constraint for the automatic search of endmembers in hyperspectral data. *Sensors*, (8): 1321—1342

附中文参考文献

褚海峰，翟中敏，赵银锑，李平湘，张良培. 2007. 一种多/高光谱遥感图像端元提取的凸锥分析算法. 遥感学报，**11**(4): 460—467